Developmental Cell *10*, 81–92, January, 2006 ©2006 Elsevier Inc. DOI 10.1016/j.devcel.2005.12.002

Dose-Dependent Interaction of *Tbx1* and *Crkl* and Locally Aberrant RA Signaling in a Model of *del22q11* Syndrome

Deborah L. Guris,[1,2] Gregg Duester,[3] Virginia E. Papaioannou,[4] and Akira Imamoto[1,2,*]

[1]The Ben May Institute for Cancer Research and Center for Molecular Oncology

[2]Committee on Developmental Biology
The University of Chicago
Chicago, Illinois 60637

[3]OncoDevelopmental Biology Program
The Burnham Institute
La Jolla, California 92037

[4]Department of Genetics and Development
College of Physicians and Surgeons
Columbia University
New York, New York 10032

Summary

22q11 deletion (*del22q11*) syndrome is characterized genetically by heterozygous deletions within chromosome 22q11 and clinically by a constellation of congenital malformations of the aortic arch, heart, thymus, and parathyroid glands described as DiGeorge syndrome (DGS). Here, we report that compound heterozygosity of mouse homologs of two 22q11 genes, *CRKL* and *TBX1*, results in a striking increase in the penetrance and expressivity of a DGS-like phenotype compared to heterozygosity at either locus. Furthermore, we show that these two genes have critical dose-dependent functions in pharyngeal segmentation, patterning of the pharyngeal apparatus along the anteroposterior axis, and local regulation of retinoic acid (RA) metabolism and signaling. We can partially rescue one salient feature of DGS in *Crkl*$^{+/-}$;*Tbx1*$^{+/-}$ embryos by genetically reducing the amount of RA produced in the embryo. Thus, we suggest that *del22q11* is a contiguous gene syndrome involving dose-sensitive interaction of *CRKL* and *TBX1* and locally aberrant RA signaling.

Introduction

Abnormal development of a transient embryonic structure known as the pharyngeal apparatus has been implicated in the pathogenesis of DGS (Larsen, 2001; Lindsay, 2001). This structure, which arises during midgestation, consists of reiterated pharyngeal arches separated medially by endodermal pouches and laterally by ectodermal clefts. In humans and mice, there are five pharyngeal arches (numbered 1–4 and 6) and four pharyngeal pouches. Neural crest cells migrate from the hindbrain into distinct pharyngeal arches and are thought to convey positional information to the arches from their rhombomere of origin (Trainor and Krumlauf, 2001). Segmentation of the arches, however, is dependent upon the pharyngeal endoderm, and the importance of interactions between these two tissues in patterning the vertebrate head has become increasingly clear (Piotrowski and Nusslein-Volhard, 2000). Experimental disruption of numerous developmental pathways affecting either the neural crest or the pharyngeal endoderm has been shown to recapitulate a DGS phenotype in model organisms.

Deletions on human chromosome 22 are the leading cause of DGS in humans. Nearly 90% of *del22q11* patients share a 3 Mb deletion at 22q11.2, while 8% harbor a smaller 1.5 Mb deletion in the centromeric half of the 3 Mb region (reviewed by Lindsay, 2001; Scambler, 2000). The remainder are characterized by smaller "atypical" deletions (reviewed by Lindsay, 2001; Scambler, 2000; Yamagishi and Srivastava, 2003). An unsolved question regarding 22q11 deletions is whether the associated congenital defects are caused by loss of a single dose-dependent 22q11 gene or rather by the combined loss of multiple linked genes that may act in a common pathway or in parallel during a critical period of pharyngeal development. Evidence supporting the idea that multiple 22q11 genes may be dose dependent comes from patients with nonoverlapping deletions within the 3 Mb region that have been reported to have a similar spectrum of defects (Baldini, 2002). Direct experimental evidence from animal models that would support the hypothesis that *del22q11* is a contiguous gene syndrome, however, has been lacking.

Mice homozygous for null alleles of the homologs of either of two 22q11 genes, *TBX1* or *CRKL*, each phenocopy multiple aspects of DGS (Guris et al., 2001; Jerome and Papaioannou, 2001; Lindsay et al., 2001; Merscher et al., 2001). The T box gene *TBX1* is located within the 1.5 Mb deletion, whereas the adaptor-protein-encoding gene *CRKL*, though it resides outside the 1.5 Mb deletion, is located within the common 3 Mb deletion as well as an atypical deletion on the distal half of 22q11 (Guris et al., 2001; Lindsay, 2001; Yamagishi and Srivastava, 2003). *Tbx1* has been identified as the dose-dependent gene responsible for great vessel malformations that occur with partial penetrance in two chromosomal deletion models of *del22q11* engineered in the mouse, *Df1* and *Lgdel*, and a small subset of *Tbx1*$^{+/-}$ mice has been reported to develop mild malformations of the great vessels (Jerome and Papaioannou, 2001; Lindsay et al., 2001; Merscher et al., 2001). However, these defects in *Tbx1*$^{+/-}$ mice generally occur in the absence of malformations of the heart, thymus, or parathyroid glands (Jerome and Papaioannou, 2001; Merscher et al., 2001), suggesting that haploinsufficiency of *Tbx1* alone cannot account for the full spectrum of defects seen in the majority of *del22q11* patients (Merscher et al., 2001; Scambler, 2000). *Crkl* is located outside of the chromosome 16 region deleted in the *Df1* and *Lgdel* mutants (Guris et al., 2001; Lindsay et al., 1999; Merscher et al., 2001; loci information obtained at Mouse Genome Resources, www.ncbi.nlm.nih.gov/genome/guide/mouse/). Although *Crkl*$^{+/-}$ mice are generally normal, we have noted that in the C57BL/6

*Correspondence: aimamoto@uchicago.edu

background a small number of *Crkl*$^{+/-}$ embryos develop craniofacial and thymic anomalies, signifying that in certain circumstances *Crkl* is also dose sensitive (Figure S1; see the Supplemental Data available with this article online). *Crkl* is expressed ubiquitously and is highly abundant in the pharyngeal region, neural tissues, and neural crest derivatives (Guris et al., 2001), while *Tbx1* is expressed in the pharyngeal endoderm, ectoderm, and mesenchyme (Lindsay et al., 2001; Merscher et al., 2001).

In general, the spectrum of defects seen in *del22q11* patients with the common 3 Mb deletion or the smaller deletions is the same; however, there is wide variability in the severity and penetrance of characteristic defects (from clinically silent to life threatening) even in patients with identical deletions (Emanuel et al., 1999; Lindsay, 2001; Scambler, 2000). One hypothesis to explain this variability is that genetic modifiers located outside 22q11 strongly affect phenotypic penetrance and expressivity. A few studies have identified modifiers that enhance the phenotype of model organisms lacking *Tbx1* (Stalmans et al., 2003; Vitelli et al., 2002). In the accompanying manuscript (Moon et al., 2006), we show that reduced dosage of one such modifier, *Fgf8*, enhances the heterozygous and homozygous phenotype of *Crkl* mutants as well. These results suggest that common pathways may link multiple 22q11 genes during critical stages of embryogenesis.

It is also known that either deficiency or excess vitamin A and its biologically active derivative, retinoic acid (RA), is detrimental to pharyngeal development and causes a DGS phenotype in humans and rodents (Mulder et al., 1998; Niederreither et al., 2003; Vermot et al., 2003). Therefore, genes involved in RA metabolism or signaling are candidate modifiers of the DGS phenotype associated with loss of *Crkl* or *Tbx1* in the mouse or 22q11 deletions in the human. To date, however, a direct link between the RA signaling pathway and the pathogenesis of DGS associated with 22q11 deletions has not been experimentally demonstrated.

In this report, we show that compound heterozygosity of *Crkl* and *Tbx1* in the mouse leads to a DGS phenotype comprised of aortic arch, thymic, and parathyroid defects with striking penetrance. We demonstrate that these two genes play critical roles in pharyngeal segmentation and patterning, and we show that RA signaling is ectopically activated in embryos lacking *Crkl* and/or *Tbx1* in a dose-dependent manner. We determined that the gain of function in RA signaling correlates with local changes in the expression of genes encoding enzymes that synthesize and degrade RA in single and compound mutant embryos. Furthermore, by genetically reducing the amount of RA produced in *Crkl*$^{+/-}$;*Tbx1*$^{+/-}$ embryos, we show that the penetrance of thymic defects, a salient feature of DGS, can be dramatically reduced. These results provide compelling evidence to suggest that, in the majority of cases, *del22q11* is a contiguous gene syndrome in which dose-sensitive interaction of *CRKL* and *TBX1* plays a major role. In addition, our findings suggest that local loss of retinoid homeostasis and aberrant RA signaling resulting from the reduced dosage of *CRKL* and *TBX1* is a critical step in the pathogenesis of DGS associated with 22q11 deletions.

Results

Crkl and *Tbx1* Genetically Interact

To test the hypothesis that *Crkl* and *Tbx1* may interact genetically during pharyngeal development, we generated *Crkl*$^{+/-}$;*Tbx1*$^{+/-}$ embryos with null alleles of both genes in either the *trans* or *cis* configuration on mouse chromosome 16. We found that compound heterozygosity of both *Crkl* and *Tbx1* in either configuration recapitulates thymic, parathyroid, and cardiovascular defects characteristic of DGS at a penetrance far greater than that generated by heterozygosity of *Crkl* or *Tbx1* alone. A total of 30 out of 35 *Crkl*$^{+/-}$;*Tbx1*$^{+/-}$ compound heterozygotes examined by gross dissection at E16.5 and P2 exhibited thymic defects, including bilateral hypoplasia as well as unilateral ectopic or missing lobes (Figures 1F and 1G; Table 1). Nearly 100% of these same *Crkl*$^{+/-}$;*Tbx1*$^{+/-}$ compound heterozygotes (34 out of 35 examined) had abnormalities of the great vessels, including interrupted aortic arch type B, interrupted cervical aortic arch, interrupted right retro-esophageal aortic arch, and aberrant emergence of the right subclavian artery (Figures 1C–1E; Table 1). Most cases of right subclavian artery anomalies involved distal emergence of this artery from the right common carotid artery. It is noteworthy that great vessel defects in 60% of *Crkl*$^{+/-}$;*Tbx1*$^{+/-}$ embryos were bilateral. Consistent with previous reports, 28% (5/18) of *Tbx1*$^{+/-}$ embryos had great vessel defects limited to either the right or the left side, and in only one case was thymic hypoplasia also observed (Figure 1B; Table 1). No abnormalities were found in 21 wild-type or 15 *Crkl*$^{+/-}$ heterozygotes. (Figure 1A; Table 1). Approximately 25% of *Crkl*$^{+/-}$;*Tbx1*$^{+/-}$ embryos evaluated by histological sections also had ventricular septal defects accompanied by an overriding aorta (Figures 1H and 1I), both components of tetralogy of Fallot, a constellation of heart defects often associated with 22q11 deletions (Botto et al., 2003). In addition, we observed parathyroid aplasia in 90% of *Crkl*$^{+/-}$;*Tbx1*$^{+/-}$ embryos evaluated by histological sections (11/20 unilateral and 7/20 bilateral cases) (Figures 1J and 1K). Likewise, development of parathyroid primordia, assayed by expression of *Gcm2* (Gordon et al., 2001; Gunther et al., 2000) in the third pharyngeal pouch at E10.5, was impaired in 13 out of 14 *Crkl*$^{+/-}$;*Tbx1*$^{+/-}$ embryos (Figures 1L and 1M).

Consistent with the incidence of lethal defects observed in *Crkl*$^{+/-}$;*Tbx1*$^{+/-}$ embryos, we found that recovery of postnatal *cis*-*Crkl*$^{+/-}$;*Tbx1*$^{+/-}$ pups from *cis*-*Crkl*$^{+/-}$;*Tbx1*$^{+/-}$ × C57BL/6 breeding pairs maintained in our colony was significantly reduced compared to the recovery of wild-type pups from the same breeder parents (142 wild-type versus 97 *cis*-*Crkl*$^{+/-}$;*Tbx1*$^{+/-}$ pups recovered, p = 0.0036). *Crkl*$^{-/-}$;*Tbx1*$^{-/-}$ embryos generated by timed mating of *cis*-*Crkl*$^{+/-}$;*Tbx1*$^{+/-}$ animals were present at the expected Mendelian ratio at E10.5; however, they die shortly thereafter (data not shown).

Impaired Development of the Fourth Pharyngeal Arch Artery in *Crkl*$^{+/-}$;*Tbx1*$^{+/-}$ Embryos

Aortic arch malformations in *Crkl*$^{+/-}$;*Tbx1*$^{+/-}$ compound heterozygotes were traced to impaired development of the fourth pharyngeal arch artery. The great vessels of

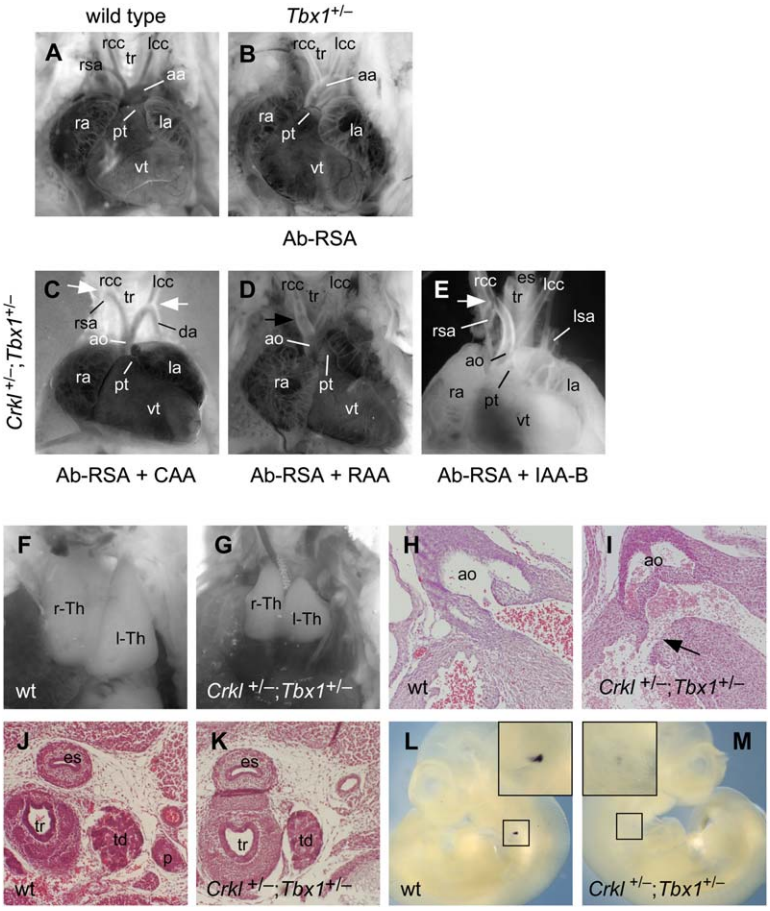

Figure 1. Aortic Arch, Thymic, and Parathyroid Defects in *Crkl*$^{+/-}$;*Tbx1*$^{+/-}$ Compound Heterozygotes

(A) Gross anatomy of the aortic arch and associated vessels in an E16.5 wild-type embryo.

(B) Aberrant origin of the right subclavian artery in a *Tbx1* heterozygote at E16.5.

(C–E) *Crkl*$^{+/-}$;*Tbx1*$^{+/-}$ embryos at E16.5 displayed fourth arch artery defects such as (C) cervical aortic arch, (D) right retro-esophageal aortic arch, (E) interrupted aortic arch type B, and (C–E) aberrant origin of the right subclavian artery. (C and E) The white arrows show the origin of either the right subclavian artery or the descending aorta. (D) The black arrow shows the origin of a right-sided arch connecting to the descending aorta behind the esophagus.

(F and G) Thymus in (F) wild-type and (G) *Crkl*$^{+/-}$;*Tbx1*$^{+/-}$ embryos at P2. Thymic lobes in compound heterozygotes were bilaterally hypoplastic compared to wild-type controls and were often located ectopically behind the vessels of the aortic arch in compound heterozygotes.

(H and I) Histological sections of the heart in a (H) wild-type and (I) *Crkl*$^{+/-}$;*Tbx1*$^{+/-}$ embryo at E16.5. A ventricular septal defect (indicated by the black arrow) accompanied by an overriding aorta is present in the (I) *Crkl*$^{+/-}$;*Tbx1*$^{+/-}$ embryo.

(J and K) The development of parathyroid glands was assessed in histological sections in (J) wild-type and (K) *Crkl*$^{+/-}$;*Tbx1*$^{+/-}$ embryos. Parathyroid glands were unilaterally or bilaterally absent in the majority of *Crkl*$^{+/-}$;*Tbx1*$^{+/-}$ embryos.

(L and M) Expression of the parathyroid primordium marker *Gcm2* in the third pharyngeal pouch of (L) wild-type and (M) *Crkl*$^{+/-}$;*Tbx1*$^{+/-}$ embryos at E10.5. The inset shows an enlargement of the third pharyngeal pouch.

Ab-RSA, aberrant origin of the right subclavian artery; ao, aorta; CAA, cervical aortic arch; da, descending aorta; es, esophagus; IAA-B, interrupted aortic arch type B; pt, pulmonary trunk; RAA, right retro-esophageal aortic arch; ra and la, right or left atrium; rcc and lcc, right or left common carotid artery; rsa and lsa, right or left subclavian artery; r-Th and l-Th, right or left thymic lobe; tr, trachea; vt, ventricle; es, esophagus; tr, trachea; td, thyroid gland; p, parathyroid gland.

the mature aortic arch begin as bilaterally symmetric arteries that run through the pharyngeal arches connecting the aortic sac to the dorsal aorta (Larsen, 2001). By E10.5 in mice, arteries have formed in pharyngeal arches 3, 4, and 6 that will soon undergo a process of asymmetrical remodeling to give rise to the aortic arch seen in the adult. The left fourth arch artery will form the arch of aorta connecting the ventral and left dorsal aortas, while the right fourth arch artery will form the proximal right subclavian artery, and the third arch arteries will become the left and right common carotid arteries. When examined between E10.5 and E11.0, wild-type and *Crkl*$^{+/-}$ embryos had bilaterally formed the third, fourth, and sixth arch arteries, whereas in most *Crkl*$^{+/-}$;*Tbx1*$^{+/-}$ embryos the fourth arch artery was absent (Table 2; Figures S2A, S2B, S2E, and S2F). In the remaining *Crkl*$^{+/-}$;*Tbx1*$^{+/-}$ embryos as well as most *Tbx1* heterozygotes, the fourth arch artery was hypoplastic (Table 2; Figures S2C and S2D) (Jerome and Papaioannou, 2001; Morishima et al., 2003; Vitelli et al., 2002). The majority of *Tbx1*$^{+/-}$ embryos appear to recover from this early defect and form a normal aortic arch (Jerome and Papaioannou, 2001; Lindsay, 2001; Lindsay and Baldini, 2001). The increased incidence and expressivity of aortic arch malformations seen in older *Crkl*$^{+/-}$;*Tbx1*$^{+/-}$ mutants compared to *Tbx1*$^{+/-}$ embryos correlates well with the comparative penetrance and severity of fourth arch artery defects observed in these embryos at E10.5 (Tables 1 and 2). The incidence of bilateral defects and arch artery aplasia is significantly greater in *Crkl*$^{+/-}$;*Tbx1*$^{+/-}$ embryos at this stage. Remodeling of the arch arteries is also abnormal in *Crkl*$^{+/-}$;*Tbx1*$^{+/-}$ embryos assessed at E11.5 (Figures S2G and S2H).

Tbx1 and Crkl Each Play Dose-Dependent Roles in Pharyngeal Segmentation

We hypothesized that the absence of the fourth pharyngeal arch artery in *Crkl*$^{+/-}$;*Tbx1*$^{+/-}$ embryos may be due to impaired development of the fourth arch itself. *Pax1* is a marker of the pharyngeal pouches that separate the pharyngeal arches (Neubuser et al., 1995). Analysis of *Pax1* expression revealed four distinct pharyngeal pouches separating five pharyngeal arches in wild-type embryos at E10.5 (Figure 2A). In contrast, in stage-matched *Crkl*$^{+/-}$;*Tbx1*$^{+/-}$ embryos, the fourth pouch was absent or severely hypoplastic (Figure 2E),

Table 1. DiGeorge-like Defects in *Crkl*$^{+/-}$;*Tbx1*$^{+/-}$ Compound Heterozygotes

	Abnormal/ Total[a]	IAA-B[b]	RAA[c]	CAA	Ab-RSA	HT[d]	Vessel and Thymic Defects[e]
trans-Crkl$^{+/-}$;*Tbx1*$^{+/-}$	16[f]/16	1	1	6	16	14 (5)	14[g]
cis-Crkl$^{+/-}$;*Tbx1*$^{+/-}$	18[f]/19	2	6 (3)	2	18	14 (2)	14[g]
Tbx1$^{+/-}$	6/18	0	0	1	4	2	1
Crkl$^{+/-}$	0/15	0	0	0	0	0	0
Wild-type	0/21	0	0	0	0	0	0

[a] Animals between E16.5 and P2 were dissected to record morphological anomalies. Abnormal embryos were scored by the presence of either great vessel or thymic defects. The number of cases with each anomaly is shown. IAA-B, interrupted aortic arch type B; RAA, retro-oesophageal right aortic arch; CAA, cervical aortic arch; Ab-RSA, aberrant origin of right subclavian artery; HT, hypoplastic thymic lobes.
[b] IAA-B cases shown here exclude cases with RAA.
[c] RAA cases shown here are without a normal left-sided aortic arch; the number in parentheses indicates cases in which double aortic arch forms a complete vascular ring. These three cases are in addition to the six cases of RAA.
[d] HT cases shown in parentheses are embryos with an ectopic thymic lobe. All cases of ectopic thymus were hypoplastic. One case each in *trans-* and *cis-Crkl*$^{+/-}$;*Tbx1*$^{+/-}$ groups had a missing lobe (data not shown).
[e] The number of embryos that exhibit both great vessel and thymic malformations is shown.
[f] Significantly different from the *Tbx1*$^{+/-}$ group (Fisher's exact test, $p < 0.00011$).
[g] Significantly different from the *Tbx1*$^{+/-}$ group (Fisher's exact test, $p < 0.00003$).

suggesting that the caudal two pharyngeal arches fuse and that a distinct fourth arch fails to form in these embryos. We found that in *Tbx1*$^{+/-}$ embryos the fourth pouch was hypoplastic (Figure 2B), whereas in *Tbx1*$^{-/-}$ mutants only the first pharyngeal pouch formed as previously reported (Figure 2C) (Jerome and Papaioannou, 2001). Although *Crkl*$^{+/-}$ embryos appeared normal, the formation of the fourth pouch was mildly impaired in a subset of *Crkl*$^{-/-}$ embryos (Figure 2D). In addition, in approximately 15% of *Crkl*$^{-/-}$ embryos recovered at E10.5, fusion of the first and second pharyngeal arches was observed (data not shown). All pharyngeal pouches failed to form in embryos lacking both copies of *Tbx1* and *Crkl* (Figure 2F), suggesting that both these genes play critical, dose-dependent roles in pouch formation.

Altered Pharyngeal Patterning in *Crkl*;*Tbx1* Mutants

In addition to the defects in caudal pharyngeal arch formation, we found that regional patterning is disturbed in the absence of *Crkl* and *Tbx1*. Spatial restriction of *Hox* genes imparts positional identity along the anteroposterior (AP) axis. While no differences were detected in the expression of numerous *Hox* genes (including *Hoxb1*, *Hoxb3*, *Hoxb4*, and *Hoxd4*) between single *Crkl* or *Tbx1* heterozygotes and wild-type embryos, ectopic anterior expression of these genes was consistently observed in the pharyngeal region of *Crkl*$^{+/-}$;*Tbx1*$^{+/-}$ as well as *Tbx1* single and *Crkl*$^{-/-}$;*Tbx1*$^{-/-}$ embryos compared to controls at E10.5. The ectopic anterior expression of these *Hox* genes suggests that pharyngeal tissues are abnormally posteriorized in mutant embryos. Interestingly, these patterning defects appear to be restricted to the pharyngeal region, as marker expression for all genes examined was normal in the hindbrain and trunk of mutant embryos.

Expression of *Hoxb1*, which normally is restricted to the endoderm and mesoderm caudal to pouch 4 in wild-type embryos at E10.5, was adjacent to the third pouch in *Crkl*$^{+/-}$;*Tbx1*$^{+/-}$ embryos (Figures 3A and 3B); however, the size of the expression domain was unchanged. In addition, ectopic anterior expression of *Hoxb1* was observed in the pharyngeal endoderm of *Tbx1*$^{-/-}$ and *Crkl*$^{-/-}$;*Tbx1*$^{-/-}$ embryos (Figure 3C). In wild-type embryos, *Hoxb3* is normally expressed in pharyngeal pouches 3 and 4 and in the mesenchyme of pharyngeal arches 3, 4, and 6. In *Crkl*$^{+/-}$;*Tbx1*$^{+/-}$ embryos, this general pattern of expression is maintained; however, caudal streams of neural crest expressing *Hoxb3* appear to fuse in the absence of a distinct fourth pharyngeal arch and there is a striking increase in *Hoxb3* expression in the third pharyngeal pouch and the surrounding mesenchyme (Figures 3D and 3E).

Table 2. Incidence of Fourth Pharyngeal Arch Artery Defects in *Crkl*$^{+/-}$;*Tbx1*$^{+/-}$ Compound Heterozygous Embryos

		Right Fourth PAA		Left Fourth PAA			
	Abnormal/Total[a]	Absent	Hypoplastic	Absent	Hypoplastic	Bilateral Cases[b]	Cases with Absent Fourth PAA[c]
Crkl$^{+/-}$;*Tbx1*$^{+/-}$	25/25	20	4	14	9	22[d] (12[e])	22[d]
Tbx1$^{+/-}$	13/15	2	9	2	4	4 (1)	3
Crkl$^{+/-}$	0/10	0	0	0	0	0	0
Wild-type	1/24	0	1	0	0	0	0

[a] Embryos were examined by intracardiac ink injection at E10.75–11.0. Abnormal embryos are scored by the presence of either hypoplastic or absent fourth pharyngeal arch arteries (PAAs).
[b] The number of embryos with bilaterally abnormal (hypoplastic or absent) fourth PAAs. The numbers in parentheses indicate cases of bilaterally missing fourth PAAs.
[c] The number of embryos with a missing fourth PAA on one or both sides.
[d] Significantly different from that of the *Tbx1*$^{+/-}$ group (Fisher's exact test, $p < 0.00015$).
[e] Significantly different from that of the *Tbx1*$^{+/-}$ group (Fisher's exact test, $p = 0.0128$).

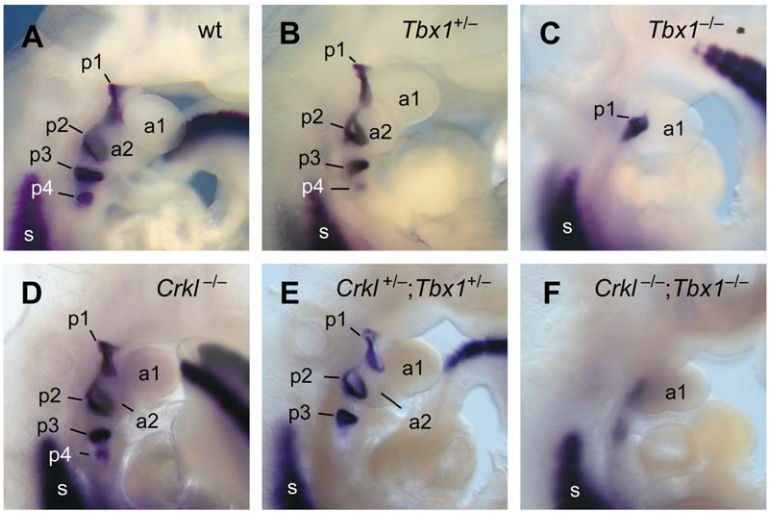

Figure 2. Pharyngeal Pouch Development in Wild-Type and Mutant Embryos

(A–F) Endodermal pouch formation was assessed by expression of *Pax1* detected by in situ hybridization at E10.5 (~34–38 somites). (A) Pharyngeal pouches 1–4 were present bilaterally in 12 wild-type embryos. (B) The fourth pharyngeal pouch was bilaterally hypoplastic in 7/8 $Tbx1^{+/-}$ embryos. In 1/8 embryos, the fourth pouch was unilaterally absent (data not shown). (C) Only the first pharyngeal pouch is formed in $Tbx1^{-/-}$ embryos. (D) The fourth pharyngeal pouch was hypoplastic in 6/6 $Crkl^{-/-}$ embryos. In two cases, this defect was bilateral, and, in four instances, it was unilateral. (E) The fourth pharyngeal pouch was absent in 16/16 $Crkl^{+/-}$;$Tbx1^{+/-}$ compound heterozygotes. In 9/16 heterozygotes, the defect was bilateral, whereas, in 7/16, the fourth pouch was absent on one side and hypoplastic on the other. (F) No pharyngeal pouches were present in 4/4 $Crkl^{-/-}$;$Tbx1^{-/-}$ double homozygous embryos, although the first arch forms and *Pax1* expression is detected in the pharyngeal endoderm. a, arch; p, pharyngeal pouch; s, somite.

In the hindbrain, expression of *Hoxb4* and *Hoxd4* begins at the rhombomere 6/7 boundary. In the pharyngeal region, we have noted that *Hoxb4* and *Hoxd4* expression appears restricted to the pharyngeal endoderm and mesenchyme caudal to the fourth pharyngeal pouch and is normally excluded from the fourth pharyngeal arch in wild-type embryos at E10.5 (Figures 3F and 3I). Ectopic expression of *Hoxb4* and *Hoxd4* in the mesenchyme and endoderm caudal to the third pouch was observed in $Crkl^{+/-}$;$Tbx1^{+/-}$ embryos at E10.5 (Figures 3G and 3J), although expression in the hindbrain was normal. This ectopic expression was expanded anteriorly in the pharyngeal endoderm of $Tbx1^{-/-}$ and $Crkl^{-/-}$;$Tbx1^{-/-}$ embryos and was observed in neural crest migrating adjacent to the rhombomere 6/7 boundary in these mutants (Figures 3H and 3K). The functional significance of observed changes in *Hox* gene expression in mutant embryos and whether such changes are primary or secondary to defects in pharyngeal segmentation are questions currently under investigation.

Locally Aberrant RA Signaling in *Crkl* and *Tbx1* Mutants

It has experimentally been shown that a gain of function in RA signaling can lead to defects in pharyngeal segmentation and a DGS phenotype in mice (Ross et al., 2000; Vermot et al., 2003). Furthermore, *Hoxb1*, *Hoxb3*, *Hoxb4*, and *Hoxd4* are known transcriptional targets of RA (Bel-Vialar et al., 2002; Folberg et al., 1999; Rossant et al., 1991). Although their expression is not wholly dependent on RA, RA is required for the normal expression of these *Hox* genes, and exogenous RA treatment has been shown to induce ectopic expression of these targets in the hindbrain (*Hoxb1*, *Hoxb3*, *Hoxb4*, and *Hoxd4*) and the pharyngeal endoderm (*Hoxb1*) (Bel-Vialar et al., 2002; Folberg et al., 1999; Matt et al., 2003; Wendling et al., 2000). Thus, the ectopic anterior expression of these RA target genes observed in the pharyngeal region of $Crkl^{+/-}$;$Tbx1^{+/-}$ as well as $Tbx1^{-/-}$ and $Crkl^{-/-}$;$Tbx1^{-/-}$ embryos is consistent with the hypothesis that RA signaling is ectopically activated in these mutants.

To further explore this possibility, we examined the expression of another known transcriptional target of RA, *Rarb*, the gene encoding the RA receptor β. In wild-type embryos at E10.5, expression of *Rarb* is restricted in the pharyngeal region to the endoderm and mesoderm caudal to the fourth pharyngeal arch and a small site of expression in the epithelia between the first and second arches (Figure 4A). In $Crkl^{+/-}$;$Tbx1^{+/-}$ embryos, expression of *Rarb* is enhanced between the first and second arches and is found adjacent to the third pharyngeal pouch in the pharyngeal endoderm (Figure 4B). Dramatic anterior expansion of *Rarb* expression is observed in the pharyngeal endoderm of $Tbx1^{-/-}$ and $Crkl^{-/-}$;$Tbx1^{-/-}$ embryos (Figures 4C and 4D). In $Crkl^{-/-}$;$Tbx1^{-/-}$ embryos, ectopic expression was also observed in the maxillary and mandibular portions of the first pharyngeal arch as well as the frontonasal mass (Figure 4D). Similar changes in the expression of *Rarb* were observed in $Tbx1^{-/-}$ and $Crkl^{-/-}$;$Tbx1^{-/-}$ embryos at E9.5 (data not shown).

To further test the hypothesis that there is a local gain of function in RA signaling in the absence of *Crkl* and *Tbx1*, we introduced a *RARE* reporter transgene consisting of a canonical RA response element followed by the *hsp68* promoter and the *LacZ* gene into mutant and control embryos. The pattern of β-galactosidase activity at a given stage assessed by incubating embryos with a colorimetric substrate is thought to reflect the distribution of RA at that time (Rossant et al., 1991), thus allowing us to qualitatively assess the levels and pattern of RA in the pharyngeal region of mutant embryos. At E10.5, ectopic reporter activity was observed in the head mesoderm of $Crkl^{-/-}$ embryos compared to wild-type controls when the colorimetric reaction was allowed to proceed overnight (Figures 4E and 4F). Similar ectopic reporter activity was observed in the head

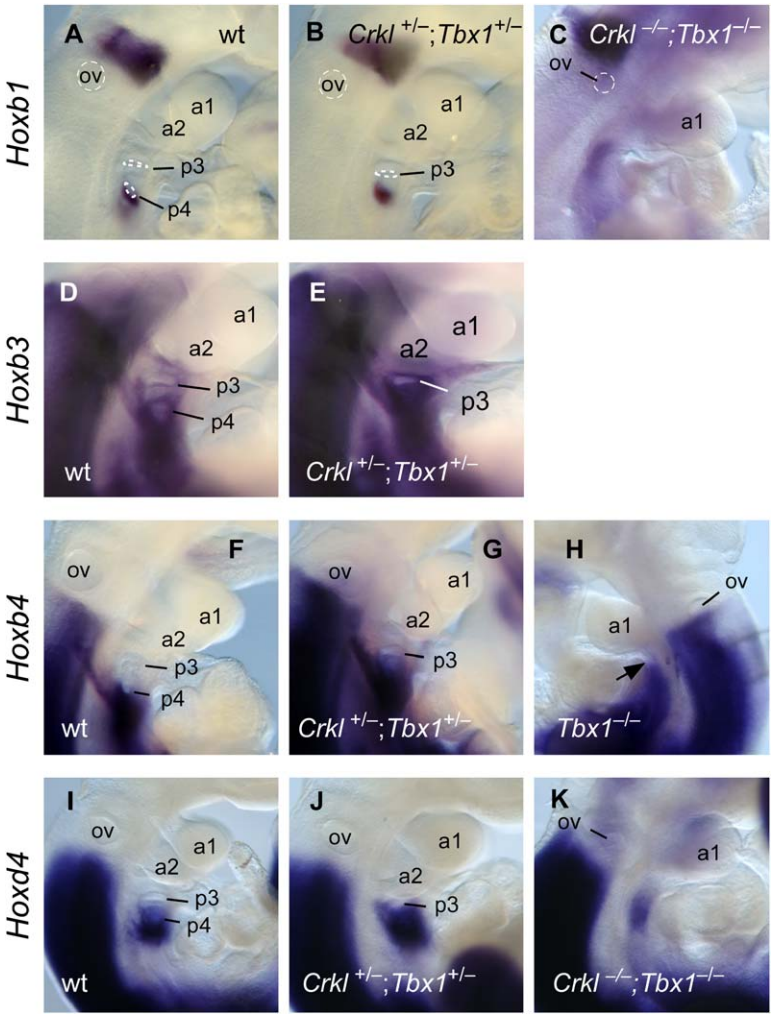

Figure 3. Altered Pharyngeal Patterning in Mutant Embryos

(A–C) *Hoxb1* expression detected by RNA in situ hybridization in (A) wild-type, (B) *Crkl*$^{+/-}$;*Tbx1*$^{+/-}$, and (C) *Crkl*$^{-/-}$;*Tbx1*$^{-/-}$ embryos at E10.5.

(D and E) *Hoxb3* expression detected by RNA in situ hybridization in (D) wild-type and (E) *Crkl*$^{+/-}$;*Tbx1*$^{+/-}$ embryos at E10.5.

(F–H) *Hoxb4* expression detected by RNA in situ hybridization in (F) wild-type, (G) *Crkl*$^{+/-}$;*Tbx1*$^{+/-}$, and (H) *Tbx1*$^{-/-}$ embryos at E10.5. *Hoxb4* expression is expanded anteriorly in the pharyngeal endoderm in *Tbx1*$^{-/-}$ embryos ([H], indicated by the black arrow) and is detected in the neural crest immediately adjacent to rhombomere 7. *Hoxb4* expression in *Crkl*$^{-/-}$;*Tbx1*$^{-/-}$ double homozygous mutants is identical to that of *Tbx1*$^{-/-}$ embryos (data not shown).

(I–K) *Hoxd4* expression detected by RNA in situ hybridization in (I) wild-type, (J) *Crkl*$^{+/-}$;*Tbx1*$^{+/-}$, and (K) *Crkl*$^{-/-}$;*Tbx1*$^{-/-}$ embryos at E10.5. *Hoxd4* expression in *Tbx1*$^{-/-}$ embryos (data not shown) is identical to that of *Crkl*$^{-/-}$;*Tbx1*$^{-/-}$ embryos. a, pharyngeal arch; ov, otic vesicle; p, pharyngeal pouch.

mesoderm of *Tbx1* homozygous mutants as well as in the pharyngeal endoderm of these embryos (Figure 4G). This ectopic reporter activity was enhanced in stage-matched *Crkl*$^{-/-}$;*Tbx1*$^{-/-}$ embryos in these tissues at this stage and was also observed in the hindbrain (Figure 4H). An abnormal pattern of RA distribution and signaling was already apparent in *Tbx1*$^{-/-}$ and *Tbx1*$^{-/-}$;*Crkl*$^{-/-}$ embryos in the head mesoderm as well as ventral pharyngeal tissues at E9.0 (Figures 4K and 4N). While no significant differences in the pattern of reporter activity were detected in *Crkl*$^{+/-}$;*Tbx1*$^{+/-}$ embryos compared to single heterozygous embryos or wild-type under these conditions at E10.5 (data not shown), subtle differences in the anterior limit of *RARE* reporter expression in the head mesoderm were detected between *Crkl*$^{+/-}$;*Tbx1*$^{+/-}$ embryos compared to wild-type controls at E9.0 (Figures 4L, 4M, and 4I). *RARE* reporter expression in *Crkl*$^{-/-}$ embryos was comparable to wild-type controls at E9.0 (Figures 4J and 4I).

Local Changes in the Expression of Genes Involved in RA Metabolism in *Crkl*;*Tbx1* Mutants

We hypothesized that the apparent local gain of function in RA signaling observed in embryos lacking *Crkl* and/or *Tbx1* may be due to local defects in retinoid metabolism that result in abnormally high levels of RA and/or an abnormal pattern of RA distribution in these mutants. In the embryo, enzymes known as retinaldehyde dehydrogenases (Raldh) catalyze a key step in the conversion of retinol to RA (Ross et al., 2000). A class of cytochrome P450 enzymes encoded by *Cyp26* genes, in turn, catabolize RA (Abu-Abed et al., 2002; Sakai et al., 2004). *Raldh* and *Cyp26* genes are expressed in complementary patterns during embryogenesis, and together their products act to ensure stereotypic levels of RA in specific tissues and a reproducible pattern of RA signaling in the developing embryo.

We first examined the expression pattern of *Raldh2*, which encodes the major enzyme responsible for production of RA in the developing embryo (Niederreither et al., 1999, 2002; Ross et al., 2000), in wild-type and mutant embryos. In the pharyngeal region of wild-type embryos, *Raldh2* expression at E10.5 is restricted to a site of posterior mesoderm caudal to the pharyngeal arches (Figure 4O). In *Tbx1*$^{-/-}$ and *Crkl*$^{-/-}$;*Tbx1*$^{-/-}$ embryos, dramatic anterior expansion of this expression domain in the pharyngeal mesoderm was observed, while the expression pattern of *Raldh2* elsewhere in the embryo was unchanged (Figures 4Q and 4R). Similar changes in the expression of *Raldh2* were observed at E9.5 in

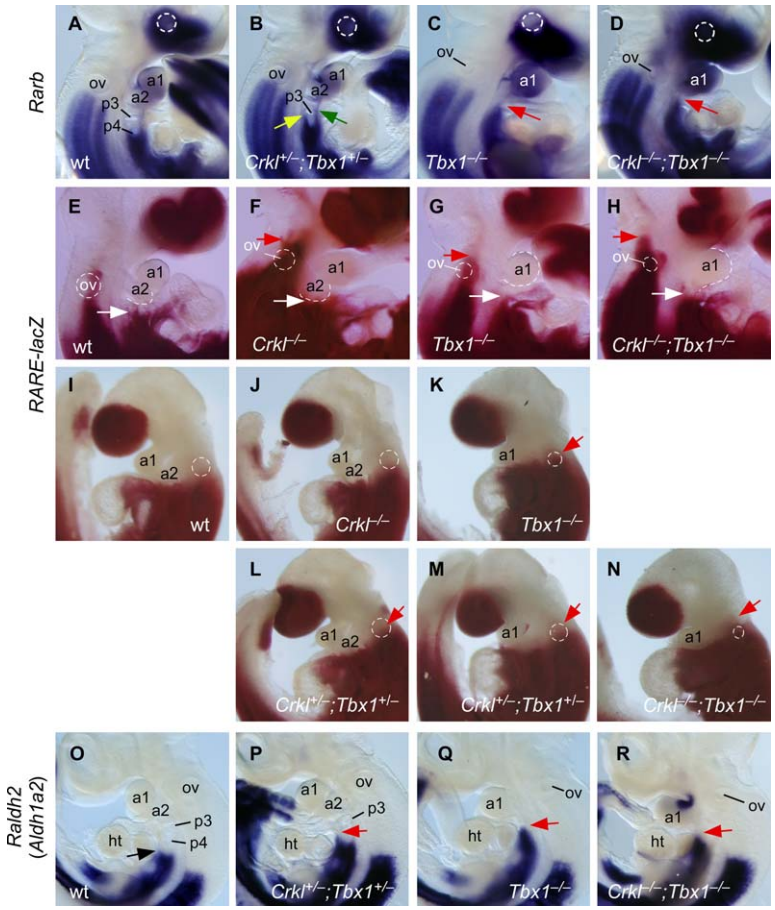

Figure 4. Altered RA Signaling in Mutant Embryos

(A–D) *Rarb* expression detected by in situ hybridization in (A) wild-type, (B) *Crkl*$^{+/-}$;*Tbx1*$^{+/-}$, (C) *Tbx1*$^{-/-}$, and (D) *Crkl*$^{-/-}$;*Tbx1*$^{-/-}$ embryos at E10.5. The green and yellow arrows in (B) and the red arrow in (C) and (D) denote abnormal anterior limits of *Rarb* expression in the pharyngeal endoderm in these mutants. See text for details.

(E–H) *RARE-lacZ* expression detected by assessing β-galactosidase activity in (E) wild-type, (F) *Crkl*$^{-/-}$, (G) *Tbx1*$^{-/-}$, and (H) *Crkl*$^{-/-}$;*Tbx1*$^{-/-}$ embryos at E10.5. The white arrows denote the anterior limit of reporter expression in the pharyngeal endoderm. Note the endodermal staining in (H) that approaches the first pharyngeal arch. (F–H) The red arrows indicate ectopic reporter activity in the head mesoderm.

(I–N) *RARE-lacZ* expression detected by assessing β-galactosidase activity in (I) wild-type, (J) *Crkl*$^{-/-}$, (D) *Tbx1*$^{-/-}$, (L and M) *Crkl*$^{+/-}$;*Tbx1*$^{+/-}$, and (N) *Crkl*$^{-/-}$;*Tbx1*$^{-/-}$ embryos at E9.0. The position of otic vesicles is marked by dotted circles. Note that the anterior limit of RARE reporter (red arrows) in the head mesoderm overlaps with the position of the otic vesicles in *Tbx1*$^{-/-}$, *Crkl*$^{+/-}$;*Tbx1*$^{+/-}$, and *Crkl*$^{-/-}$;*Tbx1*$^{-/-}$ embryos, suggesting more anterior localization of an RA gradient compared to wild-type embryos.

(O–R) *Raldh2* expression detected by in situ hybridization in (O) wild-type, (P) *Crkl*$^{+/-}$;*Tbx1*$^{+/-}$, (Q) *Tbx1*$^{-/-}$, and (R) *Crkl*$^{-/-}$;*Tbx1*$^{-/-}$ embryos at E10.5. The red arrow in (P) indicates ectopic anterior expression of *Raldh2* nearing pharyngeal pouch 3 and the cardiac outflow tract in the ventral mesoderm. Compare with the anterior limit of expression in the ventral mesoderm of the wild-type control indicated by the black arrow in (O). The red arrows in (Q) and (R) indicate dramatic anterior expansion of *Raldh2* expression in the pharyngeal mesoderm. The staining in the first pharyngeal arch in (R) is a reflection of the slightly older stage of this embryo and is not abnormal.

a, pharyngeal arch; ov, otic vesicle; p, pharyngeal pouch.

these mutants (data not shown). In *Crkl*$^{+/-}$;*Tbx1*$^{+/-}$ embryos, subtle ectopic anterior expression of *Raldh2* in the ventral pharyngeal mesoderm was observed at E10.5 (Figure 4P). We currently cannot distinguish whether there is an anterior expansion of the *Raldh2* expression domain in *Crkl*$^{+/-}$;*Tbx1*$^{+/-}$ embryos, or whether, instead, the ectopic expression observed is secondary to morphological defects in fourth pharyngeal arch formation in these mutants. In either case, we speculate that this ectopic location of a major source of RA close to the third pharyngeal pouch may disturb the normal pattern of RA signaling in the pharyngeal region and have detrimental consequences for the development of structures afflicted in DGS that may be sensitive to levels of RA. No differences in *Raldh2* expression in *Crkl*$^{-/-}$, *Crkl*$^{+/-}$, or *Tbx1*$^{+/-}$ embryos were found at this stage (data not shown).

Next, we examined the expression of *Cyp26a1* and *Cyp26b1*, genes encoding the two major RA-degrading enzymes in the pharyngeal region, in mutant embryos at E9.5 and E10.5. At these stages, *Cyp26a1* is expressed in the head mesoderm dorsal to the first three pharyngeal arches, in the ectoderm of the first pharyngeal arch and in the dorsal ectoderm of the first, second, and third pharyngeal clefts, and in the tail bud of wild-type embryos (Figures 5A and 5H) (de Roos et al., 1999). At E9.5, expression of *Cyp26a1* was notably reduced in the head mesoderm and pharyngeal ectoderm of *Crkl*$^{+/-}$;*Tbx1*$^{+/-}$ embryos; however, by E10.5, expression in these mutants was comparable to wild-type controls (Figures 5D and 5K). Expression of *Cyp26a1* was more dramatically reduced in the pharyngeal region of *Crkl* and *Tbx1* single homozygous embryos at E9.5 compared to wild-type controls, with persistent, though not complete, reduction of expression observed in these mutants at E10.5 (Figures 5E, 5F, 5L, and 5M). In *Crkl*$^{-/-}$;*Tbx1*$^{-/-}$ embryos at E9.5, no expression of *Cyp26a1* was detected in the pharyngeal region, and expression of *Cyp26a1* by E10.5 in these mutants was minimal (Figures 5G and 5N). *Cyp26a1* expression in *Tbx1*$^{+/-}$ embryos appeared to be reduced at this stage (Figure 5C), whereas *Crkl*$^{+/-}$ embryos showed no overt change (Figure 5B). In all mutants, expression of *Cyp26a1* in the tail bud appeared normal.

We similarly found local changes in the expression of *Cyp26b1* in mutant embryos compared to controls. In wild-type embryos at E9.5, *Cyp26b1* expression was detected in the hindbrain and the caudal pharyngeal endoderm (Figure 5O). By comparison, expression of *Cyp26b1* in *Crkl*$^{+/-}$;*Tbx1*$^{+/-}$ embryos appeared normal

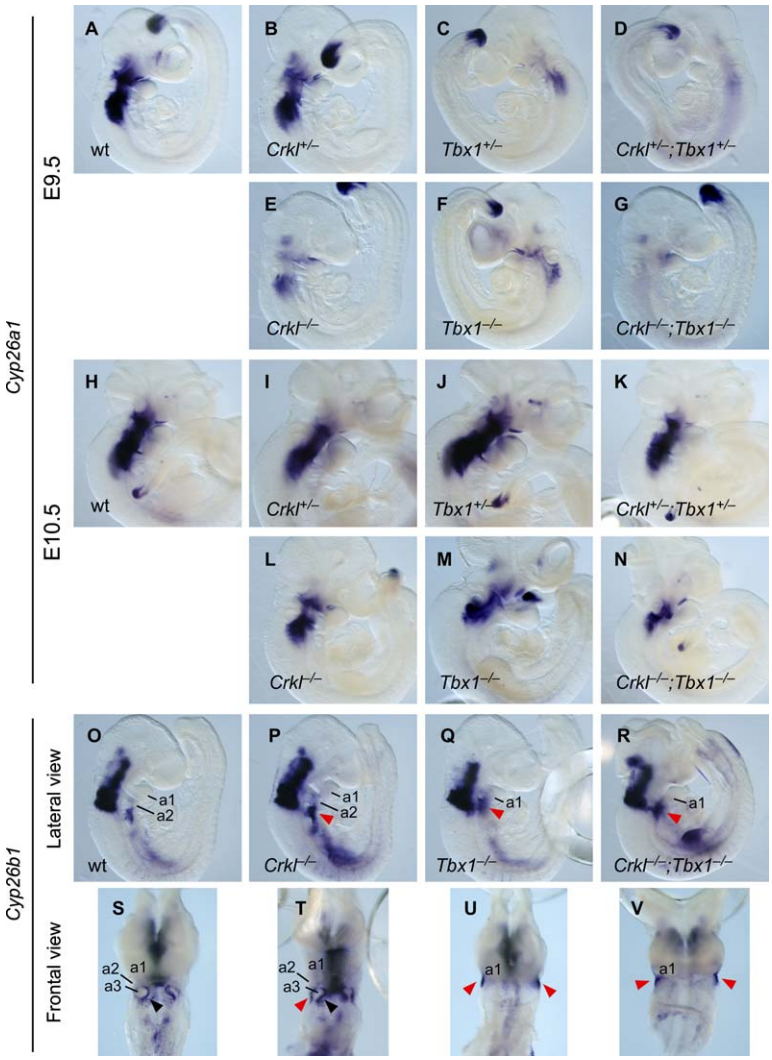

Figure 5. Altered Expression of *Cyp26* Genes in Mutant Embryos

(A–N) *Cyp26a1* expression detected by in situ hybridization at (A–G) E9.5 and (H–N) E10.5 in (A and H) wild-type, (B and I) *Crkl*$^{+/-}$, (C and J) *Tbx1*$^{+/-}$, (D and K) *Crkl*$^{+/-}$;*Tbx1*$^{+/-}$, (E and L) *Crkl*$^{-/-}$, (F and M) *Tbx1*$^{-/-}$, and (G and N) *Crkl*$^{-/-}$;*Tbx1*$^{-/-}$ embryos. See text for details.

(O–V) (O–R) Lateral and frontal views of *Cyp26b1* expression detected by in situ hybridization in (O and S) wild-type, (P and T) *Crkl*$^{-/-}$, (Q and U) *Tbx1*$^{-/-}$, and (R and V) *Crkl*$^{-/-}$;*Tbx1*$^{-/-}$ embryos at E9.5. The black arrowheads in (S) and (T) indicate expression in the endoderm lining pharyngeal arch 3. The red arrowheads in (P)–(R) and (T)–(V) indicate ectopic expression in the pharyngeal ectoderm. Frontal views were photographed after removal of the heart. See text for details.

a, pharyngeal arch.

at this stage (data not shown). However, in *Tbx1*$^{-/-}$ embryos, expression of *Cyp26b1* in the pharyngeal endoderm was reduced (Figure 5Q), while ectopic expression of this gene in the pharyngeal ectoderm adjacent to the otic placode was simultaneously observed (Figures 5Q and 5U). This ectopic expression in the ectoderm was likewise observed in *Crkl*$^{-/-}$;*Tbx1*$^{-/-}$ embryos at E9.5 (Figures 5R and 5V), and, in these mutants, the loss of *Cyp26b1* in the pharyngeal endoderm was more pronounced (Figure 5V). Ectopic expression of *Cyp26b1* in the pharyngeal ectoderm was also observed in *Crkl*$^{-/-}$ embryos (Figures 5P and 5T). Ectopic expression of *Cyp26b1* in the pharyngeal ectoderm persisted in *Tbx1*$^{-/-}$ and *Crkl*$^{-/-}$;*Tbx1*$^{-/-}$ embryos at E10.5, and ectopic expression in the anterior pharyngeal endoderm was additionally observed at this stage (data not shown).

Regulation of the expression of Cyp26 enzymes involves multiple inputs including RA (Loudig et al., 2000), and exogenous RA treatment has been shown to locally induce expression of *Cyp26a1* or *Cyp26b1* in developing embryos (Reijntjes et al., 2005; Sakai et al., 2001). We therefore postulate that the ectopic expression of *Cyp26b1* observed in the ectoderm and anterior pharyngeal endoderm of *Tbx1*$^{-/-}$ and *Crkl*$^{-/-}$;*Tbx1*$^{-/-}$ embryos, as well as the abnormal pattern of expression of *Cyp26a1* in the head mesoderm, may be due to a negative feedback mechanism triggered by aberrant RA signaling in these embryos.

Gain of Function in RA Signaling Contributes to the Pathogenesis of Thymic Defects in *Crkl*$^{+/-}$;*Tbx1*$^{+/-}$ Embryos

The analysis of *Crkl* and *Tbx1* single and compound homozygous mutants that we have described suggests that there are potential changes in RA homeostasis and a local increase in RA signaling in the absence of *Crkl* and *Tbx1*. To assess the functional importance of these findings to the DGS phenotype observed in *Crkl*$^{+/-}$;*Tbx1*$^{+/-}$ mutants, we generated *Crkl*$^{+/-}$;*Tbx1*$^{+/-}$ embryos in which the gene dosage of *Raldh2* was reduced by half by timed matings between *cis*-*Crkl*$^{+/-}$;*Tbx1*$^{+/-}$ animals and mice bearing a heterozygous null mutation in *Raldh2* (Mic et al., 2002). When examined between E15.5 and E18.5 by gross dissection, we found that the penetrance of thymic hypoplasia was significantly and dramatically decreased in *Crkl*$^{+/-}$;*Tbx1*$^{+/-}$;*Raldh2*$^{+/-}$ triple heterozygous compared to

Table 3. Reduced *Raldh2* Gene Dosage Decreases the Penetrance of Thymic Defects in *Crkl*$^{+/-}$;*Tbx1*$^{+/-}$ Embryos

Genotype	Hypoplastic[a]/Total (%)
Crkl$^{+/-}$;*Tbx1*$^{+/-}$;*Raldh2*$^{+/-}$	15[b]/40 (37.5)
Crkl$^{+/-}$;*Tbx1*$^{+/-}$	23/32 (71.9)
Raldh2$^{+/-}$	0/33 (0)
Wild-type	1/25 (4)

Embryos at E15.5–E17.5 were isolated from timed mating between *cis*-*Crkl*$^{+/-}$;*Tbx1*$^{+/-}$ and *Raldh2*$^{+/-}$ parents. The variation of the thymic size (measured in terms of thymic lobe height) in wild-type and *Raldh2*$^{+/-}$ embryos was within 10% from their average, except that one wild-type embryo had a small thymic lobe that was approximately 86% of the average. Thymic lobes were scored hypoplastic if the size was smaller than 90% of the average of the control embryos in the litter. Postanalysis revealed that thymic lobes judged normal were 0.998 ± 0.062 (mean ± SD) relative to the average thymic size of the control littermates, whereas those judged hypoplastic were 0.778 ± 0.084.

[a] The number of embryos exhibiting thymic hypoplasia.

[b] Statistically different from the frequency of the *Crkl*$^{+/-}$;*Tbx1*$^{+/-}$ group (p = 0.0047, Fisher's exact test).

Crkl$^{+/-}$;*Tbx1*$^{+/-}$ embryos (Table 3). In contrast, no significant difference in the penetrance of aortic arch defects between *Crkl*$^{+/-}$;*Tbx1*$^{+/-}$ double and *Crkl*$^{+/-}$;*Tbx1*$^{+/-}$;*Raldh2*$^{+/-}$ triple heterozygous embryos was observed (Table S1). These results clearly substantiate a functionally important role for locally aberrant RA signaling in the pathogenesis of DGS associated with compound heterozygous loss of *Crkl* and *Tbx1*.

Reduced Dosage of *Fgf8* Enhances Key Features of the DGS Phenotype in *Crkl*$^{+/-}$;*Tbx1*$^{+/-}$ Mutants

In addition to the key role played by RA, Fgf signaling is also critical for pharyngeal development. *Fgf8* appears to be important for pharyngeal pouch development, pharyngeal arch artery formation, and neural crest survival (Abu-Issa et al., 2002; Frank et al., 2002), and mice bearing a hypomorphic allele of *Fgf8* in *trans* to a null *Fgf8* allele display features of DGS. Reduced dosage of *Fgf8* has been shown to increase the penetrance of aortic arch defects in *Tbx1* heterozygotes (Vitelli et al., 2002), and we have now reported that reduced dosage of *Fgf8* significantly enhances the *Crkl* mutant phenotype as well (see accompanying manuscript, Moon et al., 2006 [this issue of *Developmental Cell*]). We therefore assessed the effects of reduced gene dosage of *Fgf8* on the penetrance and expressivity of two key features of DGS found in *Crkl*$^{+/-}$;*Tbx1*$^{+/-}$ mutants. When examined by gross dissection between E15.5 and E17.5, we found that the incidence and severity of thymic defects was significantly increased in *Crkl*$^{+/-}$;*Tbx1*$^{+/-}$;*Fgf8*$^{+/-}$ triple heterozygous embryos compared to *Crkl*$^{+/-}$;*Tbx1*$^{+/-}$ mutants (Table S2). Bilateral thymic defects were observed in all *Crkl*$^{+/-}$;*Tbx1*$^{+/-}$;*Fgf8*$^{+/-}$ triple heterozygous embryos, and the severity of hypoplasia and the incidence of thymic lobe aplasia were exacerbated in embryos of this genotype. Reduced dosage of *Fgf8* likewise enhanced the severity of aortic arch defects in *Crkl*$^{+/-}$;*Tbx1*$^{+/-}$ mutants. We found that the incidence of defects likely to cause significant postnatal morbidity or neonatal lethality (IAA-B with or without a right retroesophageal arch, respectively) was significantly increased in *Crkl*$^{+/-}$;*Tbx1*$^{+/-}$;*Fgf8*$^{+/-}$ triple heterozygous compared to *Crkl*$^{+/-}$;*Tbx1*$^{+/-}$ double heterozygous mutants (Table S2).

Discussion

Dose-Sensitive Interaction of Crkl and Tbx1 Is Required for Development of Structures Afflicted in DGS

We have shown that *Crkl* and *Tbx1* both play critical, dose-dependent roles in pharyngeal segmentation and patterning, and that compound heterozygosity of these two 22q11 homologs recapitulates key features of DGS with dramatic penetrance and expressivity. Our findings suggest that development of the caudal pharyngeal apparatus is particularly sensitive to the reduced dosage of *Crkl* and *Tbx1*, as development of the fourth pharyngeal arch and its associated artery is impaired in *Crkl*$^{+/-}$;*Tbx1*$^{+/-}$ embryos. Furthermore, in this and the accompanying manuscript (Moon et al., 2006) we have linked developmental defects associated with loss of *Crkl* and *Tbx1* to two major signaling pathways (RA and Fgf8) implicated in the pathogenesis of a DGS-like phenotype in model organisms. To our knowledge, these results provide novel insight into the genetic and developmental mechanisms underlying malformations associated with 22q11 deletions in humans.

Since *Crkl* encodes an SH2-SH3-SH3 adaptor protein implicated in tyrosine kinase signaling, and *Tbx1* encodes a transcription factor, the molecular basis for the synergy observed between these two genes is not obvious. Likewise, the expression pattern of *Crkl* and *Tbx1* is quite different, as Crkl is ubiquitously expressed, while *Tbx1* is more restricted. There is mounting evidence that the severe defects observed in *Tbx1* homozygous embryos are due to the loss of *Tbx1* action in the pharyngeal endoderm (Kochilas et al., 2002; Lindsay, 2001; Merscher et al., 2001; Piotrowski et al., 2003). The expression pattern of *Crkl* and *Tbx1* overlaps in this tissue; however, Crkl protein expression is also enriched in neural crest derivatives such as smooth muscle and cranial nerves. Future studies will determine the molecular basis for the observed synergy between *Crkl* and *Tbx1* and whether these two genes act in the same cells or in different tissues (or both) during pharyngeal development and in the pathogenesis of DGS.

Implications for Human Disease: *del22q11* Is a Contiguous Gene Syndrome

Our finding that the mouse homologs of two 22q11 genes, *Tbx1* and *Crkl*, genetically interact in a dosage-sensitive manner provides compelling evidence that, in the majority of cases, DGS is a contiguous gene syndrome. The dramatic increase in the penetrance and expressivity of defects caused by compound heterozygosity of *Crkl* and *Tbx1* is consistent with the finding that the majority of patients that present with a DGS phenotype (~90%) harbor a 3 Mb deletion encompassing both *TBX1* and *CRKL*, while the occurrence of smaller or atypical deletions is quite low. No data are currently available regarding the frequency of different 22q11 deletions in the general, nonsyndromic population. Our data suggest that the propensity to develop manifestations of DGS may be increased when the dosage of

both *TBX1* and *CRKL* is reduced; however, in some instances, genetic modifiers or other factors may render development of the pharyngeal apparatus sensitive to the reduced dosage of a single 22q11 gene. For instance, our finding that reduced *Fgf8* gene dosage enhances the DGS-like phenotype of *Crkl* mutant embryos and *Crkl*$^{+/-}$;*Tbx1*$^{+/-}$ compound heterozygotes, in addition to previous work demonstrating genetic interaction between *Fgf8* and *Tbx1* (Vitelli et al., 2002), suggests that Fgf8 signaling may affect the penetrance and expressivity of specific features of DGS associated with 22q11 deletions, including either *CRKL* or *TBX1* or the common 3 Mb deletion encompassing both of these genes. In addition, the possibility remains that heterozygous deletion of other 22q11 loci may generate additional aspects of DGS, either independently or as modifiers of the reduced dosage of either or both *TBX1* and *CRKL* (Merscher et al., 2001; Scambler, 2000).

Loss of Retinoid Homeostasis and Locally Aberrant RA Signaling in Embryos Lacking *Crkl* and *Tbx1*

The importance of RA in patterning the pharyngeal endoderm is well documented, as are the teratogenic effects of RA on development of the pharyngeal apparatus (reviewed by Mark et al., 2004). Several recent studies have demonstrated that perturbation of RA signaling during embryogenesis can lead to a DGS phenotype in the mouse (Mulder et al., 1998; Niederreither et al., 2003; Vermot et al., 2003; Wendling et al., 2000). Until now, however, no study has directly linked defects in RA signaling to the pathogenesis of DGS associated with 22q11 deletions.

Our analysis of embryos lacking *Crkl* and/or *Tbx1* indicates that in the absence of these two genes there is a gain of function in RA signaling specifically in the pharyngeal region. Ectopic anterior expression of the *RARE* reporter was observed in *Crkl*$^{-/-}$, *Tbx1*$^{-/-}$, and *Crkl*$^{-/-}$;*Tbx1*$^{-/-}$ embryos, indicating that higher than normal levels and an abnormal distribution of RA are present in the pharyngeal region. In *Tbx1*$^{-/-}$ and *Crkl*$^{-/-}$;*Tbx1*$^{-/-}$ embryos, the pharyngeal endoderm is notably posteriorized, with ectopic anterior expression of multiple RA target genes (including *Hoxb1*, *Hoxb3*, *Hoxb4*, *Hoxd4*, and *Rarb*) observed. The fact that defects associated with exogenous RA exposure at earlier stages of development are not generally observed in embryos lacking *Crkl* and/or *Tbx1* suggests that the gain of function in RA signaling in these mutants is not only regionally restricted, but is potentially temporally restricted as well.

The severe defects in pharyngeal segmentation, patterning, and RA distribution observed in *Tbx1*$^{-/-}$ and *Crkl*$^{-/-}$;*Tbx1*$^{-/-}$ embryos correlate with dramatic changes in the expression pattern of *Raldh2*, *Cyp26a1*, and *Cyp26b1* in the pharyngeal region in these mutants. A recent study has also reported quantitative changes in the levels of *Raldh2* and *Cyp26a1* expressed in *Tbx1*$^{+/-}$;*Df1*$^{+/-}$ compound heterozygous mutants detected by microarray analysis (Ivins et al., 2005). Changes in the expression patterns of the *RARE* reporter or *Raldh2*, *Cyp26a1*, and *Cyp26b1* were subtle or undetectable at all stages in *Crkl*$^{+/-}$;*Tbx1*$^{+/-}$ embryos compared to wild-type controls. We speculate that some differences in the pattern and levels of gene expression and distribution of RA in *Crkl*$^{+/-}$;*Tbx1*$^{+/-}$ embryos may not readily be detected by the methods we have used in our analysis. Furthermore, even subtle differences in the stereotypic pattern of RA signaling may nonetheless be detrimental to development of caudal pharyngeal structures, as many of these structures (including the thymus and parathyroid glands) have been experimentally shown to be sensitive to excess RA (Mulder et al., 1998). Such speculation is supported by our finding that the penetrance of thymic hypoplasia is dramatically reduced in *Crkl*$^{+/-}$;*Tbx1*$^{+/-}$;*Raldh2*$^{+/-}$ triple heterozygous embryos compared to *Crkl*$^{+/-}$;*Tbx1*$^{+/-}$ mutants.

There are several possible explanations for the findings that thymic defects were not completely suppressed and that the penetrance of aortic arch defects was not significantly decreased in *Crkl*$^{+/-}$;*Tbx1*$^{+/-}$ mutants by reducing the dosage of *Raldh2*. One explanation may be that as there are changes in the expression of numerous genes involved in RA metabolism (*Raldh2*, *Cyp26a1*, *Cyp26b1*) and signaling (*Rarb*) in the absence of *Crkl* and *Tbx1*, reducing the gene dosage of *Raldh2* may not completely rescue the gain of function in RA signaling in *Crkl*$^{+/-}$;*Tbx1*$^{+/-}$ mutants to wild-type levels. An alternative, although not exclusive, explanation may be that aberrant RA signaling may be only one of multiple factors that contribute to the etiology of thymic defects and aortic arch defects in *Crkl*$^{+/-}$;*Tbx1*$^{+/-}$ embryos. The findings that Fgf8 signaling modifies the phenotype of *Crkl*$^{+/-}$;*Tbx1*$^{+/-}$ as well as *Crkl*$^{+/-}$ and *Tbx1*$^{+/-}$ mutant embryos (Moon et al., 2006; Vitelli et al., 2002) support the hypothesis that multiple factors may contribute to the pathogenesis of defects observed in *Crkl*$^{+/-}$;*Tbx1*$^{+/-}$ embryos. It will be informative to determine whether reducing the gene dosage of *Raldh2* by half suppresses other aspects of DGS observed in *Crkl*$^{+/-}$;*Tbx1*$^{+/-}$ embryos, and whether such a reduction of *Raldh2* dosage more completely rescues the milder presentation of DGS features observed in *Tbx1* single heterozygous embryos.

Complete loss of *Raldh2*, *Cyp26a1*, or *Cyp26b1* has devastating consequences for development of the tissues in which these genes are expressed, suggesting that levels of RA must be finely tuned at a local level to ensure proper development, and that Raldh and cytochrome P450 enzymes play a major role in establishing and maintaining this balance. *Tbx1* and *Crkl* may play critical, dose-sensitive roles in the temporal and spatial regulation of RA signaling in the pharyngeal region by directly or indirectly regulating the level or pattern of expression of these genes involved in RA metabolism. We therefore propose that disruption of retinoid homeostasis due to the loss of these genes is an early and important step in the pathogenesis of DGS in *del22q11*. Based on our findings, we also speculate that genes involved in RA metabolism and signaling may act as modifiers of the phenotype associated with 22q11 deletions. Furthermore, if RA production and signaling is elevated and/or occurs ectopically and the capacity to degrade RA is impaired in the absence of *Crkl* and *Tbx1*, it is also possible that levels of maternal RA or retinol exposure that are not normally teratogenic to wild-type embryos may significantly worsen the severity of defects caused by loss of these genes. Future studies will further explore the link between levels of RA signaling and the

manifestation of salient features of DGS in embryos lacking *Crkl* and *Tbx1*.

Experimental Procedures

Mice

We previously described *Tbx1* and *Crkl* null alleles, *Tbx1*^{tm1Pa} and *Crkl*^{tm1Imo}, respectively (abbreviated as *Tbx1*$^{-}$ and *Crkl*$^{-}$) (Guris et al., 2001; Jerome and Papaioannou, 2001). *Tbx1*$^{+/-}$ mice (originally generated with R1 ES cells and maintained by a 129S6/SvEvTac backcross) have been backcrossed to C57BL/6J or 129S4 inbred strains. *Crkl*$^{+/-}$ mice (originally generated in the 129S4/SvJaeSor inbred background) have been maintained by continual C57BL/6J or 129S4 backcross for more than 11 generations. Timed mating between *Tbx1*$^{+/-}$ and *Crkl*$^{+/-}$ mice in a partially mixed 129Sv;C57BL/6 background (N2-N5 toward C57BL/6) was used to obtain *trans*-compound heterozygous embryos. As *Crkl* and *Tbx1* are closely linked on mouse chromosome 16 with a physical distance of ~1.1 Mb, compound heterozygosity for *Crkl* and *Tbx1* in *cis* was generated as a result of meiotic recombination. Two *cis*-*Crkl*$^{+/-}$;*Tbx1*$^{+/-}$ compound heterozygotes out of a total of 106 pups were obtained by breeding *trans*-*Crkl*$^{+/-}$;*Tbx1*$^{+/-}$ compound heterozygotes (in a 129/Sv background) to wild-type C57BL/6 mice, while the remaining pups were heterozygous for either *Crkl* (50 pups) or *Tbx1* (54 pups) (Fisher's exact test, $p < 2.2 \times 10^{-16}$). A test cross of these compound heterozygotes with C57BL/6J wild-type mice generated 15 wild-type or 10 compound heterozygous mice, but no heterozygotes were recovered for a single locus, thus confirming that the parent genotype was indeed *cis*-compound heterozygous (Fisher's exact test, $p = 3.06 \times 10^{-7}$). Further backcross with C57BL/6 was carried out to obtain N3–N5 generations for the current studies. Double homozygous mice were obtained by intercross between *cis*-compound heterozygotes. To monitor *RARE* activities, genetic crosses were set up with the *RARE-hsp68lacZ* strain (Rossant et al., 1991; a gift from W. Cardoso, originally from J. Rossant). Heterozygosity of this reporter was identified by PCR with *hsp68F1* (5′-agacgcgaaactgctg gaagatt-3′) and *lacZR1* (5′-gctggcgaaaggggatgtgct-3′) primers. The reporter activity was assessed by using a standard protocol and the colorimetric substrate Salmon-gal (Biosynth). *Crkl*$^{+/-}$;*Tbx1*$^{+/-}$;*Raldh2*$^{+/-}$ triple heterozygous embryos were obtained by timed mating between *cis*-*Crkl*$^{+/-}$;*Tbx1*$^{+/-}$ compound heterozygotes in a C57BL/6 background (N3-N5) and *Raldh2*$^{+/-}$ heterozygotes in a mixed 129Sv;B6;Black Swiss background (Mic et al., 2002). *Crkl*$^{+/-}$;*Tbx1*$^{+/-}$;*Fgf8*$^{+/-}$ triple heterozygous embryos were generated by timed mating between *cis*-*Crkl*$^{+/-}$;*Tbx1*$^{+/-}$ compound heterozygotes in a C57BL/6 background (N3-N5) and *Fgf8*$^{+/-}$ heterozygotes in a C57BL/6 background (>N5) (a gift from Anne Moon) or by timed mating between surviving *Crkl*$^{+/-}$;*Tbx1*$^{+/-}$;*Fgf8*$^{+/-}$ triple heterozygotes with C57BL/6 wild-type animals.

Intracardiac Ink Injection

The cardiac ventricles of embryos isolated between E10.5 and E11.5 were injected with India ink through a pulled glass capillary as previously described (Guris et al., 2001; Lindsay et al., 1999). Embryos were postfixed with 4% paraformaldehyde and preserved in 70% ethanol.

In Situ RNA Hybridization

Whole-mount in situ RNA hybridization on E9.5 and E10.5 embryos was performed by using a standard protocol. RNA probes were made from plasmid templates including the following cDNA inserts: *Pax1*, *Gcm2*, *Hoxa2*, *Hoxa3*, *Hoxb3*, and *Hoxd3* (gifts from N. Manley); *Hoxd4* (a gift from M. Featherstone); *Hoxb1* and *Hoxb4* (gifts from R. Krumlauf); *Raldh2* (a gift from P. Dolle); *Cyp26a1*, *Cyp26b1*, and *Rarb* (mouse cDNA clones from Open Biosystems).

Supplemental Data

Supplemental Data including Crkl haploinsufficiency, intracardiac ink injections, the spectrum of great vessel defects in *Crkl*$^{+/-}$;*Tbx1*$^{+/-}$;*Raldh2*$^{+/-}$ embryos, and exacerbated vascular and thymic defects in *Crkl*$^{+/-}$;*Tbx1*$^{+/-}$;*Fgf8*$^{+/-}$ embryos are available at http://www.developmentalcell.com/cgi/content/full/10/1/81/DC1/.

Acknowledgments

We thank W. Cardoso, P. Dolle, M. Featherstone, R. Krumlauf, N. Manley, A. Moon, and J. Rossant for reagents; N. Williams and C. Bowers for excellent technical assistance; and the members of the Imamoto Lab, D. Ahn, E. Ferguson, E. Grove, R. Ho, E. McNally, and V. Prince for critical reading of the manuscript. We are very grateful to E. Ferguson, N. Manley, and V. Prince for fruitful discussions concerning aspects of this work. D.L.G was supported by the Developmental Pediatrics Training Grant from the National Institutes of Health (T32HD007009). This work was supported in part by grants from the National Institutes of Health (R01GM062848 to G.D.; R01HD033082 to V.E.P.; and R01DE015883 to A.I.). The authors declare that they have no competing financial interests.

Received: August 12, 2005
Revised: November 17, 2005
Accepted: December 6, 2005
Published: January 9, 2006

References

Abu-Abed, S., MacLean, G., Fraulob, V., Chambon, P., Petkovich, M., and Dolle, P. (2002). Differential expression of the retinoic acid-metabolizing enzymes CYP26A1 and CYP26B1 during murine organogenesis. Mech. Dev. *110*, 173–177.

Abu-Issa, R., Smyth, G., Smoak, I., Yamamura, K.I., and Meyers, E.N. (2002). Fgf8 is required for pharyngeal arch and cardiovascular development in the mouse. Development *129*, 4613–4625.

Baldini, A. (2002). DiGeorge syndrome: the use of model organisms to dissect complex genetics. Hum. Mol. Genet. *11*, 2363–2369.

Bel-Vialar, S., Itasaki, N., and Krumlauf, R. (2002). Initiating Hox gene expression: in the early chick neural tube differential sensitivity to FGF and RA signaling subdivides the HoxB genes in two distinct groups. Development *129*, 5103–5115.

Botto, L.D., May, K., Fernhoff, P.M., Correa, A., Coleman, K., Rasmussen, S.A., Merritt, R.K., O'Leary, L.A., Wong, L.Y., Elixson, E.M., et al. (2003). A population-based study of the 22q11.2 deletion: phenotype, incidence, and contribution to major birth defects in the population. Pediatrics *112*, 101–107.

de Roos, K., Sonneveld, E., Compaan, B., ten Berge, D., Durston, A.J., and van der Saag, P.T. (1999). Expression of retinoic acid 4-hydroxylase (CYP26) during mouse and *Xenopus laevis* embryogenesis. Mech. Dev. *82*, 205–211.

Emanuel, B.S., Budarf, M.L., and Scambler, P.J. (1999). The genetic basis of conotruncal cardiac defects: the chromosome 22q11.2 deletion. In Heart Development, R.P. Harvey, and N. Rosenthal, eds. (San Diego: Academic Press), pp. 463–478.

Folberg, A., Nagy Kovacs, E., Luo, J., Giguere, V., and Featherstone, M.S. (1999). RARβ mediates the response of Hoxd4 and Hoxb4 to exogenous retinoic acid. Dev. Dyn. *215*, 96–107.

Frank, D.U., Fotheringham, L.K., Brewer, J.A., Muglia, L.J., Tristani-Firouzi, M., Capecchi, M.R., and Moon, A.M. (2002). An Fgf8 mouse mutant phenocopies human 22q11 deletion syndrome. Development *129*, 4591–4603.

Gordon, J., Bennett, A.R., Blackburn, C.C., and Manley, N.R. (2001). Gcm2 and Foxn1 mark early parathyroid- and thymus-specific domains in the developing third pharyngeal pouch. Mech. Dev. *103*, 141–143.

Gunther, T., Chen, Z.F., Kim, J., Priemel, M., Rueger, J.M., Amling, M., Moseley, J.M., Martin, T.J., Anderson, D.J., and Karsenty, G. (2000). Genetic ablation of parathyroid glands reveals another source of parathyroid hormone. Nature *406*, 199–203.

Guris, D.L., Fantes, J., Tara, D., Druker, B.J., and Imamoto, A. (2001). Mice lacking the homologue of the human 22q11.2 gene *CRKL* phenocopy neurocristopathies of DiGeorge syndrome. Nat. Genet. *27*, 293–298.

Ivins, S., Lammerts van Beuren, K., Roberts, C., James, C., Lindsay, E., Baldini, A., Ataliotis, P., and Scambler, P.J. (2005). Microarray analysis detects differentially expressed genes in the pharyngeal region of mice lacking Tbx1. Dev. Biol. *285*, 554–569.

Jerome, L.A., and Papaioannou, V.E. (2001). DiGeorge syndrome phenotype in mice mutant for the T-box gene, Tbx1. Nat. Genet. *27*, 286–291.

Kochilas, L., Merscher-Gomez, S., Lu, M.M., Potluri, V., Liao, J., Kucherlapati, R., Morrow, B., and Epstein, J.A. (2002). The role of neural crest during cardiac development in a mouse model of DiGeorge syndrome. Dev. Biol. *251*, 157–166.

Larsen, W.J. (2001). Human Embryology, Third Edition (New York: Churchill Livingstone).

Lindsay, E.A. (2001). Chromosomal microdeletions: dissecting *del22q11* syndrome. Nat. Rev. Genet. *2*, 858–868.

Lindsay, E.A., and Baldini, A. (2001). Recovery from arterial growth delay reduces penetrance of cardiovascular defects in mice deleted for the DiGeorge syndrome region. Hum. Mol. Genet. *10*, 997–1002.

Lindsay, E.A., Botta, A., Jurecic, V., Carattini-Rivera, S., Cheah, Y.C., Rosenblatt, H.M., Bradley, A., and Baldini, A. (1999). Congenital heart disease in mice deficient for the DiGeorge syndrome region. Nature *401*, 379–383.

Lindsay, E.A., Vitelli, F., Su, H., Morishima, M., Huynh, T., Pramparo, T., Jurecic, V., Ogunrinu, G., Sutherland, H.F., Scambler, P.J., et al. (2001). Tbx1 haploinsufficiency in the DiGeorge syndrome region causes aortic arch defects in mice. Nature *410*, 97–101.

Loudig, O., Babichuk, C., White, J., Abu-Abed, S., Mueller, C., and Petkovich, M. (2000). Cytochrome P450RAI(CYP26) promoter: a distinct composite retinoic acid response element underlies the complex regulation of retinoic acid metabolism. Mol. Endocrinol. *14*, 1483–1497.

Mark, M., Ghyselinck, N.B., and Chambon, P. (2004). Retinoic acid signalling in the development of branchial arches. Curr. Opin. Genet. Dev. *14*, 591–598.

Matt, N., Ghyselinck, N.B., Wendling, O., Chambon, P., and Mark, M. (2003). Retinoic acid-induced developmental defects are mediated by RARβ/RXR heterodimers in the pharyngeal endoderm. Development *130*, 2083–2093.

Merscher, S., Funke, B., Epstein, J.A., Heyer, J., Puech, A., Lu, M.M., Xavier, R.J., Demay, M.B., Russell, R.G., Factor, S., et al. (2001). TBX1 is responsible for cardiovascular defects in velo-cardio-facial/DiGeorge syndrome. Cell *104*, 619–629.

Mic, F.A., Haselbeck, R.J., Cuenca, A.E., and Duester, G. (2002). Novel retinoic acid generating activities in the neural tube and heart identified by conditional rescue of Raldh2 null mutant mice. Development *129*, 2271–2282.

Moon, A.M., Guris, D.L., Seo, J.-H., Li, L., Hammond, J., Talbot, A., and Imamoto, A. (2006). Crkl deficiency disrupts Fgf8 signaling in a mouse model of 22q11 deletion syndromes. Dev. Cell *10*, this issue, 71–80.

Morishima, M., Yanagisawa, H., Yanagisawa, M., and Baldini, A. (2003). Ece1 and Tbx1 define distinct pathways to aortic arch morphogenesis. Dev. Dyn. *228*, 95–104.

Mulder, G.B., Manley, N., and Maggio-Price, L. (1998). Retinoic acid-induced thymic abnormalities in the mouse are associated with altered pharyngeal morphology, thymocyte maturation defects, and altered expression of Hoxa3 and Pax1. Teratology *58*, 263–275.

Neubuser, A., Koseki, H., and Balling, R. (1995). Characterization and developmental expression of Pax9, a paired-box-containing gene related to Pax1. Dev. Biol. *170*, 701–716.

Niederreither, K., Subbarayan, V., Dolle, P., and Chambon, P. (1999). Embryonic retinoic acid synthesis is essential for early mouse post-implantation development. Nat. Genet. *21*, 444–448.

Niederreither, K., Vermot, J., Fraulob, V., Chambon, P., and Dolle, P. (2002). Retinaldehyde dehydrogenase 2 (RALDH2)- independent patterns of retinoic acid synthesis in the mouse embryo. Proc. Natl. Acad. Sci. USA *99*, 16111–16116.

Niederreither, K., Vermot, J., Le Roux, I., Schuhbaur, B., Chambon, P., and Dolle, P. (2003). The regional pattern of retinoic acid synthesis by RALDH2 is essential for the development of posterior pharyngeal arches and the enteric nervous system. Development *130*, 2525–2534.

Piotrowski, T., and Nusslein-Volhard, C. (2000). The endoderm plays an important role in patterning the segmented pharyngeal region in zebrafish (Danio rerio). Dev. Biol. *225*, 339–356.

Piotrowski, T., Ahn, D.G., Schilling, T.F., Nair, S., Ruvinsky, I., Geisler, R., Rauch, G.J., Haffter, P., Zon, L.I., Zhou, Y., et al. (2003). The zebrafish van gogh mutation disrupts tbx1, which is involved in the DiGeorge deletion syndrome in humans. Development *130*, 5043–5052.

Reijntjes, S., Blentic, A., Gale, E., and Maden, M. (2005). The control of morphogen signalling: regulation of the synthesis and catabolism of retinoic acid in the developing embryo. Dev. Biol. *285*, 224–237.

Ross, S.A., McCaffery, P.J., Drager, U.C., and De Luca, L.M. (2000). Retinoids in embryonal development. Physiol. Rev. *80*, 1021–1054.

Rossant, J., Zirngibl, R., Cado, D., Shago, M., and Giguere, V. (1991). Expression of a retinoic acid response element-hsplacZ transgene defines specific domains of transcriptional activity during mouse embryogenesis. Genes Dev. *5*, 1333–1344.

Sakai, Y., Meno, C., Fujii, H., Nishino, J., Shiratori, H., Saijoh, Y., Rossant, J., and Hamada, H. (2001). The retinoic acid-inactivating enzyme CYP26 is essential for establishing an uneven distribution of retinoic acid along the anterio-posterior axis within the mouse embryo. Genes Dev. *15*, 213–225.

Sakai, Y., Luo, T., McCaffery, P., Hamada, H., and Drager, U.C. (2004). CYP26A1 and CYP26C1 cooperate in degrading retinoic acid within the equatorial retina during later eye development. Dev. Biol. *276*, 143–157.

Scambler, P.J. (2000). The 22q11 deletion syndromes. Hum. Mol. Genet. *9*, 2421–2426.

Stalmans, I., Lambrechts, D., De Smet, F., Jansen, S., Wang, J., Maity, S., Kneer, P., von der Ohe, M., Swillen, A., Maes, C., et al. (2003). VEGF: a modifier of the *del22q11* (DiGeorge) syndrome? Nat. Med. *9*, 173–182.

Trainor, P.A., and Krumlauf, R. (2001). Hox genes, neural crest cells and branchial arch patterning. Curr. Opin. Cell Biol. *13*, 698–705.

Vermot, J., Niederreither, K., Garnier, J.M., Chambon, P., and Dolle, P. (2003). Decreased embryonic retinoic acid synthesis results in a DiGeorge syndrome phenotype in newborn mice. Proc. Natl. Acad. Sci. USA *100*, 1763–1768.

Vitelli, F., Taddei, I., Morishima, M., Meyers, E.N., Lindsay, E.A., and Baldini, A. (2002). A genetic link between Tbx1 and fibroblast growth factor signaling. Development *129*, 4605–4611.

Wendling, O., Dennefeld, C., Chambon, P., and Mark, M. (2000). Retinoid signaling is essential for patterning the endoderm of the third and fourth pharyngeal arches. Development *127*, 1553–1562.

Yamagishi, H., and Srivastava, D. (2003). Unraveling the genetic and developmental mysteries of 22q11 deletion syndrome. Trends Mol. Med. *9*, 383–389.